Computer Aided Brain Tumor Diagnosis using Coati Optimization Algorithm with Explainable Artificial Intelligence Approach

Wajdi Alghamdi[1,*]

[1]Department of Information Technology, Faculty of Computing and Information Technology, King Abdulaziz University, Jeddah, 21589, Saudi Arabia
Emails: wmalghamdi@kau.edu.sa

Abstract

Brain tumors (BT) are a difficult and dangerous medical condition, and the accurate and early analysis of these tumors is crucial for suitable treatment. Explainability in clinical image diagnosis role a vital play in the correct analysis and treatment of tumors that supports medical staff's optimum understanding of the image analysis performances rely upon deep methods. Artificial intelligence (AI), in certain deep neural networks (DNNs) has attained remarkable outcomes for clinical image analysis in many applications. However, the need for explainability of deep neural approaches has been assumed that major restriction before executing these approaches in medical practice. Explainable AI, or XAI, is a vital module in this context as it supports medical staff and patients in understanding the AI's decision-making model, enhancing trust and transparency. It leads to optimum patient care and performance but making sure that medical staff can make learned decisions depends on AI-driven insights. Therefore, this study develops a novel Computer-Aided Brain Tumor Diagnosis using Coati Optimization Algorithm with an Explainable Artificial Intelligence (CABTD-COAXAI) approach. The purpose of the CABTD-COAXAI technique is to exploit XAI and hyperparameter-tuned deep learning (DL) approaches for automated BT analysis. To accomplish this, the CABTD-COAXAI technique follows a Gaussian filtering (GF) based noise removal process. Besides, the CABTD-COAXAI technique utilizes the EfficientNetB7 methods for the feature extraction process. Additionally, the hyperparameter tuning of the EfficientNetB7 method is performed by the use of COA. Furthermore, the classification of the BT process can be performed by the usage of a convolutional autoencoder (CAE). Finally, the CABTD-COAXAI system combines the XAI method named LIME to effectively understand and explainability of the black-box model for automated BT diagnosis. The simulation result of the CABTD-COAXAI technique has been tested on a benchmark BT database. The extensive outcomes inferred that the CABTD-COAXAI method reaches superior performance over other models in terms of different measures

Keywords: Explainable Artificial Intelligence; Brain tumour; Convolutional Autoencoder; LIME; Coati Optimization Algorithm

1. Introduction

Tumors are exposed to human health for extremely long periods. Malignant brain tumors (BT) like glioblastoma can have a highly low rate of survival and are extremely associated with the death of young patients with BT [1]. Patients with BT generally endure chemotherapy, radiotherapy, surgery, and other treatment approaches, however, differentiating BT from the brain parenchyma can be visually Complex. The process requires to be sensibly treated for finding and removing cancers via surgery [2]. Medical specialists commonly conduct analysis first employing image analysis technologies namely nuclear magnetic resonance imaging (MRI), computed tomography (CT), and electroencephalogram (EEG), as well as support in finding the diseased region and boundaries via imaging software [3]. Computer-aided diagnosis (CAD) systems depend on MRI have produced huge amounts of images that could be utilized for evaluating or classifying the lesion region in detail. CADs have been diagnosed and visualized different structures of the human brain like the BT boundary and blood–brain barrier [4]. However,

DOI: https://doi.org/10.54216/FPA.170203
Received: January 16, 2024 Revised: April 12, 2024 Accepted: September 13, 2024

medical research workers must be focused on a sequence of issues like lower clarity and contrast, when processing a massive amount of medical images owing to the difficulty of manual retrieval of MRI images as well as the requirement for classification [5]. If these issues are successfully addressed relevant physician treatment techniques and decision-making strategies. Once these MRI orders can be automatically identified by machine learning (ML), consequently, if the tumour presents itself, a medical specialist is more rapidly confirmed, thus analysing and classifying if it is required [6].

In the gradual development of artificial intelligence (AI) and interdisciplinary technologies, deep architectures are progressively implemented in different medical image functions, particularly in brain science research [7]. By comparison with natural scene images, medical image data instances can be typically low, which results in numerous limits in real-time applications. Current growths in the domain of AI, specifically deep learning (DL) are promoted to improved attention for diagnosing BT that causes and their diverse growth stages. With medical applications, there have been usually some data instances with great difficulty in contrast to other applications [8]. However, the advent of DL methods in the medical field has still been confined because of some limitations [9]. In complex applications like brain imaging applications, this can be vital to comprehend the aim behind the predictive network to confirm that the architecture offers accurate evaluation. Consequently, explainable AI (XAI) has attained considerable attention for analyzing the "black box" DL networks in the health domain [10]. XAI techniques permit research workers, end-users, and developers to achieve transparent DL algorithms, which could determine their solution to humans in a comprehensible way. For medical end-users, the requirement for interpretability has been increased in producing their reliance on DL methods and promoting them to implement these models for supporting medical measures.

This study develops a novel Computer-Aided Brain Tumor Diagnosis using the Coati Optimization Algorithm with an Explainable Artificial Intelligence (CABTD-COAXAI) approach. The purpose of the CABTD-COAXAI technique is to exploit XAI and hyperparameter-tuned deep learning models for automated BT diagnosis. To accomplish this, the CABTD-COAXAI technique follows a Gaussian filtering (GF) based noise removal process. Besides, the CABTD-COAXAI approach utilizes the EfficientNetB7 methods for the feature extraction method. Additionally, the hyperparameter tuning of the EfficientNetB7 method is performed by the usage of COA. Furthermore, the classification of the BT process can be performed by the usage of a convolutional autoencoder (CAE). Finally, the CABTD-COAXAI approach combines the XAI approach named LIME to effectively understand and explainability of the black-box model for automated BT diagnosis. The simulation result of the CABTD-COAXAI technique is tested on a benchmark BT database.

2. Related Works

In [11], the authors considered the binary classification of brain images acquired from MRI images of the human being's brain from various viewpoints in addition to an appropriate interpretation of the forecast outcomes. This developed classification method dependent upon the notion of DTL employing a pre-trained VGG-16 architecture and "Image Net" weights for automatically removing features at the inputs of MRI images. In [12], a cancer was segmented once capably pre-processing MRI. Further, the highest features are extracted by the combination of the DWT and GLCM. Lastly, the extracted features could be provided into enhanced CNNs-based classification employing a novel enhanced meta-heuristic method, termed BSSA in the last identification to increase the CNN effectiveness regarding accuracy and reliability.

Lu et al. [13] introduced an innovative CAD technique called PBTNet to diagnose earlier BT in MRIs. A pre-trained ResNet18 could be chosen as the backbone architecture in this PBTNet and then, adjusted only for extracting features. Subsequently, 3 randomized NNs namely, random vector functional-connection, Schmidt neural network, and ELM assisted as the models for PBTNet that can be trained to the features and labels. Deepak and Ameer [14] considered a 3-class classification complexity for distinguishing between glioma, pituitary, and meningioma tumors that create 3 significant categories of BT. This designed classification method accepts the notion of DTL and employs a pretrained GoogLeNet for extracting features as MRI images. Verified classifier methods could be combined for classifying the removed features.

Sadad et al. [15] implemented segmentation via the Unet model with ResNet-50 like a backbone with the Figshare database and gained about 0.9504 at the IoU. The data augmentation and preprocessing notion could be implemented to enrich the rate of classification. The multi-classification of BT was executed by exploiting evolutionary algorithms (EA) and reinforcement learning (RL) by employing TL. The authors [16] designed an innovative CNN-assisted multi-grade BT categorizing method. Initially, cancerous areas from an MRI were segmented employing a DL method. Then, wide-ranging data augmentation could be utilized for efficiently training this developed technique, preventing the shortage of information issues while managing with MRI for multi-grade categorization of BT.

DOI: https://doi.org/10.54216/FPA.170203
Received: January 16, 2024 Revised: April 12, 2024 Accepted: September 13, 2024

The authors [17] developed a technique of multi-level extraction features and considered them for earlier recognition of BT. These 2 pre-trained DL methods such as Inceptionv3 and DensNet-201 generated this model valid. With numerous Inception models, the features are primarily removed in pre-trained Inceptionv3 architecture and combined with these features for classifying BT. Secondarily; pre-trained DensNet201 could be employed in removing features from different blocks of DensNet. Afterwards, these features could be incorporated and provided for a softmax technique for classifying the BT. In [18], binary classification of healthy brain tissues and BT along with pseudo-BT was attained through DNN employing MRS data. A stacked architecture dependent upon LSTM and BiLSTM with DNNs has been established for the classification of MRI signals.

3. The Proposed Model

In this research, we concentrate on the development and design of the CABTD-COAXAI approach. The purpose of the CABTD-COAXAI technique is to exploit XAI and hyper parameter-tuned DL models for automated BT diagnosis. To accomplish this, the CABTD-COAXAI technique contains GF-pre-processing, EfficientNetB7-based feature extraction, COA-based parameter tuning, and CAE-based classification. Figure 1 demonstrates the workflow of the CABTD-COAXAI approach.

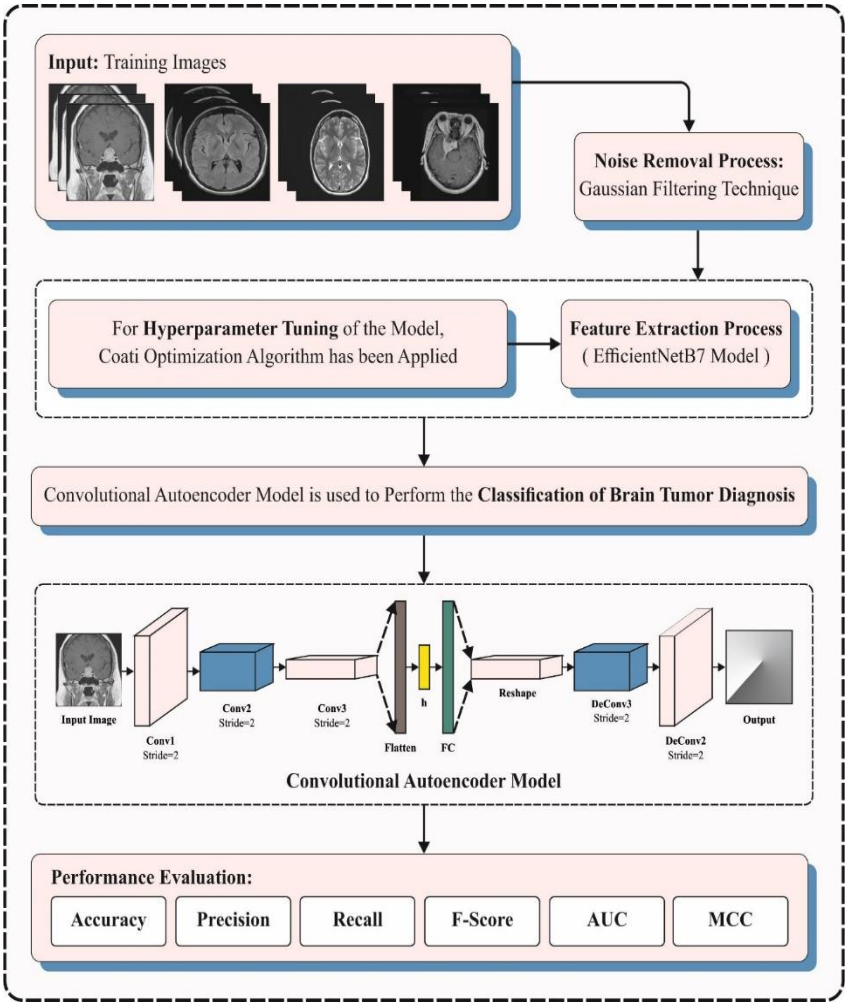

Figure 1. Workflow of CABTD-COAXAI approach

A. Image Pre-processing

Primarily, the GF-based noise removal process is a basic and effectual approach employed in image processing to better image quality by decreasing unwanted noise [19]. This method leverages a Gaussian kernel, a mathematical function considered by its bell-shaped curve that is executed to whole images. By convolving, the image with this kernel, GF smoothes the image, attenuating high-frequency noise elements but maintaining the underlying structural details. The amount of smoothing has been managed by the standard deviation (SD) parameter of the Gaussian kernel, permitting customizable noise reduction but preserving image clarity.

DOI: https://doi.org/10.54216/FPA.170203
Received: January 16, 2024 Revised: April 12, 2024 Accepted: September 13, 2024

B. Feature extraction: EfficientNetB7 model

For the process of feature extraction, the CABTD-COAXAI technique applies the EfficientNetB7 model. EfficientNetB7 is a high-precision method attained by expanding EfficientNetB0, its size of input image is 600x600, its depth multiplier factor (d) is 3.1, and its width multiplier factor (w) is 2.0 [20]. In the proposed model, EfficientNetB7 was chosen to be a benchmark model to obtain better classification performance in the rock image dataset.

The EfficientNetB7 module was constructed by stacking various modules on top of Mobile Inverted Bottleneck Convolution (MBConv). As its feature mappings of input and output are broader than the middle, the architecture of MBConv is different from the classical residual module. The MBConv modules include a Dropout layer, convolution layer of 1×1 kernel size, depthwise separable convolution, and Squeeze (SE) attention modules. After the convolution layer, The MBConv modules apply the Swish activation function and Batch Normalization (BN). The Swish activation function avoids overfitting and establishes nonlinearity to the data, whereas BN speeds up the model convergence and normalizes the data during their training. Furthermore, the SE attention model from the MBConv model integrates the SE attention module that improves the model's ability by capturing the data of channel attention from the input feature mapping.

The SE attention model was used for calculating the significance of all the channels in the input feature mapping for the existing task and weighted them. It can be obtained by the subsequent 3 operations:

- Squeeze: The feature mapping of CxHxW input size was generally average pooled into mapping feature of 1x1xC, thereby squeezing the 2D feature channels as a solitary value for representing the worldwide distribution of response on all the channels.
- Excitation: A full connection NN is utilized for converting the squeezed map, which generates activated weight by sigmoid activation and ReLU functions.
- Scale: The activated weight is employed for weighting all the channels from the input feature mapping by implementing dot multiplication.

The feature mapping of $C\times H\times W$ rock size is inputted into the SE attention model. Using these operations, the module allocates weight to all the channels based on the effect on rock image classification performance, improving rock feature channels and suppress the weaker ones. The channels from the resultant tensor have dissimilar color borders, representing weight that has been allocated to all the channels after passing by the SE model.

C. Parameter tuning: COA

The hyperparameter tuning of the EfficientNetB7 method is implemented by the usage of the COA method. COA duplicates features of coati animals [21]. COA method is assumed to reverse actual world optimization issues. Coati animals are mostly dispersed in the US and consume sound in black paws, small ears, upward direction, and tails. This animal permits signs by employing its tail. The entire extent of a grownup coati animal is between sort of 33-69 cm and weighs nearly 2-8 kilograms. Male coati animals complete double the extent of females. The coati animal consumes only foods like lizards, rats, and crocodile eggs. However, it consumes lizards as the most required food because lizards expend their maximum time on trees. Therefore, coati animals fake lizards by making a team. In this significance, they stand on top of the tree in order to grasp close to the lizard, and attempt to fall down on the lizard. By utilizing this situation, another team will start their violent procedure. Dogs, eagles, and other animals also hunt coati animals. Coatti's location is candidate performance in order to exact problems. Initialized coati animals from searching space rely on place conveyed in Eq. (1).

$$Y_a: y_{a,b} = lbound_b + s(ubound_b - lbound_b), \quad (1)$$

$$here, a = 1,2..Ob = 1,2..n$$

Here, place of coati animals at a^{th} location is signified as Y_i, the choice variable showed as n, and the amount of coati animals directed as O, judgment variable of b is designated $Y_{a,b}$, up as well as low bounds showed as $ubound_a, lbound_b$ and the random real number is signified as s between zero and one.

Arithmetic design of COA: Coati animals contain dual major features such as attacking and escaping that are explained in detail in coming fragments.

Attacking characteristics: The attacking feature is primarily employed to update the location of the coati animal's population. Here, coati animals started climbing on top of the tree in order to terror lizards so that it is fell to ground portion. At present, residual team members of coati animal hunt for lizards. In this situation, coati must be annoyed to alter location on searching space.

DOI: https://doi.org/10.54216/FPA.170203
Received: January 16, 2024 Revised: April 12, 2024 Accepted: September 13, 2024

Now, the place of the lizard can measured as the position of the optimal coati animal. In searching procedure, total team members of coati animals were separated into dual parts that are other team was positioned on the ground, and enduring team members stood on a tree in order to fear the lizard. Here, the position of coati animals fixed on the tree is recognized by Eq. (2).

$$Y_a^{q^1}: y_{a,b}^{q^1} = y_{a,b} + s\left(lizard_b - J.y_{a,b}\right),$$

$$here, a = 1,2..\frac{O}{2}b = 1,2..n \tag{2}$$

The lizards are positioned casually only after chop down procedure. A coati animal's underway movement procedure depends on lizard animals' random site that is expressed utilizing Eqs. (3), (4) and (5).

$$lizard^H : lizard_k^H = lbound_k + s(ubound_b - lbound_b), b = 1,2..n \tag{3}$$

$$Y_a^{q^1}: y_{a,b}^{q^1} = \begin{cases} y_{a,b} + s\left(lizard_b^H - J.y_{a,b}\right), G_{lizard^H} < G_a \\ y_{a,b} + s(lizard_b^H) - J.y_{a,b}), else \end{cases} \tag{4}$$

$$for\ a = \left[\frac{O}{2}\right] + 1, \left[\frac{O}{2}\right] + 2, \ldots O, and\ b = 1,2..n \tag{5}$$

If a novel location improves the main function then it is advanced. If the objective function is not improved, then the place is not promoted. The form $a = 1,2..O$ is defined through Eq. (6).

$$Y_a = \begin{cases} Y_a^{q^1} + G_a^{q^1} < G_a \\ Y_a\ else \end{cases} \tag{6}$$

Here, coati's upgrade location is specified as $Y_a^{q^1}$, random unique number denoted as s in [0,1], lizard location showed as a lizard, position and main function of lizard on ground portion is suggested as $lizard^H$, and $G_a^{q^2}$ correspondingly, integer value is designated as J in one and two, and floor function is denoted as $\lfloor \bullet \rfloor$

Escaping behaviour: The coati animal emissions from its opponents, and this conduct is employed for upgrading the position of coati animals. The coati escapes from animals such as eagles and dogs for the purpose of security, and the novel location of coati animal is nearer to the current location. Figure 2 demonstrates the steps involved in COA.

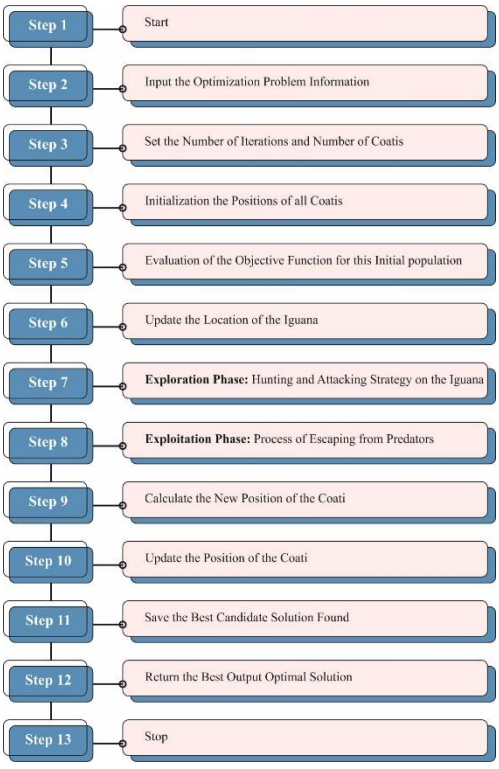

Figure 2. Steps involved in COA

DOI: https://doi.org/10.54216/FPA.170203
Received: January 16, 2024 Revised: April 12, 2024 Accepted: September 13, 2024

The coatis are situated in an arbitrary place generated near the current position of the coati animal. The casual location is formed by Eqs. (7) and (8).

$$lbound_b^{loc} = \frac{lbound_b}{u}, ubound_b^{loc} = \frac{ubound_b}{u} \tag{7}$$

$$here, u = 1,2..U$$

$$Y_a^{q^2}: y_{a,b}^{q^2} = y_{a,b} + (1-2s)\left(lbound_b^{loc}\right) + s\left(ubound_b^{loc} - lbound_b^{loc}\right), Where, a = 1,2..O, b = 1,2..n \tag{8}$$

Here, objective location is improved by a novel position, then only the original place is known and it is motivated in Eq. (9).

$$Y_a = \begin{cases} Y_a^{q^2} + G_a^{q^2} < G_a \\ Y_a \; else \end{cases} \tag{9}$$

Here, the local upper bound is $ubound_b^{loc}$ and $lbound_b^{loc}$ is a local lower bound, The innovative place of the coati animal is designated as $Y_a^{q^2}$, at b^{th} dimension, place n of coati animal is shown as $Y_{a,b}^{q^2}$, an objective function is directed as $G_a^{q^2}$, repetition counter is symbolized as U, and arbitrary quantity is denoted as S in [0,1].

The COA approach develops a fitness function (FF) for reaching a superior classification solution. It expresses a positive integer for denoting the superior efficacy of candidate outcomes. During this work, the decreasing of the classifier rate of errors can supposed to FF, as expressed in Eq. (10).

$$fitness(x_i) = ClassifierErrorRate(x_i) = \frac{No.\ of\ misclassified\ instances}{Total\ no.of\ instances} * 100 \tag{10}$$

D. Classification: CAE model

At this stage, the classification of the BT process can be performed by the usage of the CAE model. A CAE is a kind of NN that signifies the input (micro-Doppler signature for the application) from a hidden-variable space utilizing a "local" feature map generated by the convolution layer from the encoding block [22]. In the encoder, all the convolution layers following the pooling layer have been used to decrease the computation difficulty. The decoding block of CAE applies a convolutional transpose state that regenerates the input in the encoding outcome, with unpooling followed by a layer convolutional transpose state from the decoded. The architecture of CAE increases an attention layer to exploit the input dataset in its entirety to create a query, thus attaining global data that can added to the encoded outcome.

Given a single-layer CAE. Assume that hxw input image x (micro-Doppler signature together with the bias term) and P filter, the p^{th} convolution maps, o^p, is formulated by Eq. (11),

$$o^p = \sigma\left(x * \omega_e^p\right), p = 0,1,\ldots,P-1 \tag{11}$$

Now, '*' denotes the 2D convolution, σ represents the activation function, and ω_e^p indicates the p^{th} convolution filter. The output of the convolution layer is given as follows:

$$O = concat[o^0, o^{P-1}]. \tag{12}$$

In the decoder, to recreate x, a convolution transpose layer is used.

$$x' = \sigma(O * W_d), \tag{13}$$

In Eq. (13), W_d means the 2D filters of the convolution transpose layer. Unsupervised training is used to the CAE that minimizes the reconstructed error as

$$\sum_{x_i \in X} \| x_i - x_i' \|_F^2, \tag{14}$$

In Eq. (14), x_i' denotes the reconstruction version of x_i, $\| \cdot \|_F$ indicates the Frobenius norm, X shows the set of all training samples, and x_i represents the i^{th} training samples.

DOI: https://doi.org/10.54216/FPA.170203
Received: January 16, 2024 Revised: April 12, 2024 Accepted: September 13, 2024

E. XAI Approach: LIME

Finally, the CABTD-COAXAI approach combines the XAI system named LIME technique. The proposed method combines the XAI and LIME approach for optimum explainability and understanding of the Blackbox technique for the accurate detection of cancer [23]. LIME defines various ML methods for predicting regression, utilizing the featured value alteration of the data instance for transforming the featured value into the predictor support. For instance, the interpretable model in LIME is trained using small perturbation (adding random noise, eliminating particular words, and hiding part of the image) and often uses DTs or linear regression in the model. These models resolve the best part of the business victimization dataset and the quality of the above-mentioned models seems to be increasing. Likewise, there are persistent tradeoffs between interpretability and model accuracy. In general, the performance can be higher and improved by using complex approaches like random forest, call trees, material, SVM, and boosting, which are "Black-Box" methods. The LIME was used to provide a better explanation of the problems with the BlackBox classifier. The LIME is a way to understand an ML Black-Box method by seeing how prediction changes and perturbs the input data. The LIME was applied for the ML BlackBox model. The critical steps are demonstrated in the following:

A TabularExplainer can be initialized by the data applied for training based on the different class names and features.

The class explain_instance takes the reference to the sample but the explanation is crucial, along with the trained model's prediction technique and the amount of features that are added to the explanation.

4. Experimental validation

In this study, the BT detection results of the CABTD-COAXAI technique are examined on the BT MRI dataset from the Kaggle repository [24]. The dataset contains 5200 samples with four classes as represented in Table 1. Figure 3 demonstrates the sample images.

Table 1: Detailed database

Classes	No. of Instances
Glioma	1300
Meningioma	1300
No-Tumor	1300
Pituitary	1300
Total Instances	5200

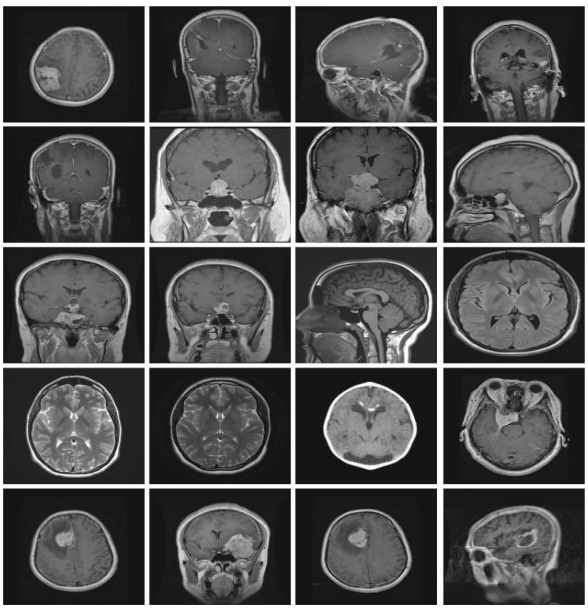

Figure 3. Sample images

DOI: https://doi.org/10.54216/FPA.170203
Received: January 16, 2024 Revised: April 12, 2024 Accepted: September 13, 2024

Figure 4 illustrates the confusion matrices attained by the CABTD-COAXAI methodology at 80:20 and 70:30 of the TRA phase/TES phase. The outcome signifies the effective detection and classification of all four classes.

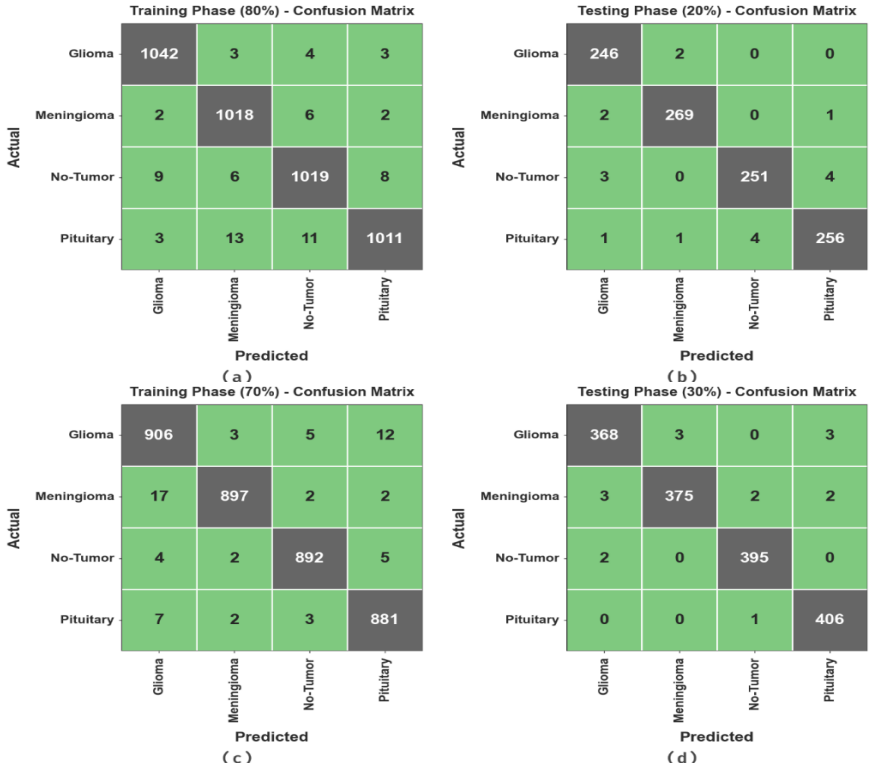

Figure 4. Confusion matrices of (a-c) TRA phase of 80% and 70% and (b-d) TES phase of 20% and 30%

The BT detection results of the CABTD-COAXAI technique are studied under 80:20 of the TRA phase/TES phase in Table 2 and Figure 5. The outcome demonstrates that the CABTD-COAXAI method gains effective performance under each class. With 80% of the TRA phase, the CABTD-COAXAI methodology provides an average $accu_y$ of 99.16%, $prec_n$ of 98.32%, $reca_l$ of 98.32%, F_{score} of 98.32%, AUC_{score} of 98.88%, and MCC of 97.76%. Meanwhile, with 20% of the TES phase, the CABTD-COAXAI system offers an average $accu_y$ of 99.13%, $prec_n$ of 98.26%, $reca_l$ of 98.27%, F_{score} of 98.26%, AUC_{score} of 98.85%, and MCC of 97.69%.

Table 2: BT detection outcome of CABTD-COAXAI technique at 80:20 of TRA phase/TES phase

Classes	$Accu_y$	$Prec_n$	$Reca_l$	F_{Score}	AUC_{Score}	MCC
TRA phase (80%)						
Glioma	99.42	98.67	99.05	98.86	99.30	98.48
Meningioma	99.23	97.88	99.03	98.45	99.16	97.94
No-Tumor	98.94	97.98	97.79	97.89	98.56	97.18
Pituitary	99.04	98.73	97.40	98.06	98.49	97.42
Average	99.16	98.32	98.32	98.32	98.88	97.76
TES phase (20%)						
Glioma	99.23	97.62	99.19	98.40	99.22	97.90
Meningioma	99.42	98.90	98.90	98.90	99.25	98.51
No-Tumor	98.94	98.43	97.29	97.86	98.39	97.16
Pituitary	98.94	98.08	97.71	97.90	98.53	97.19
Average	99.13	98.26	98.27	98.26	98.85	97.69

DOI: https://doi.org/10.54216/FPA.170203
Received: January 16, 2024 Revised: April 12, 2024 Accepted: September 13, 2024

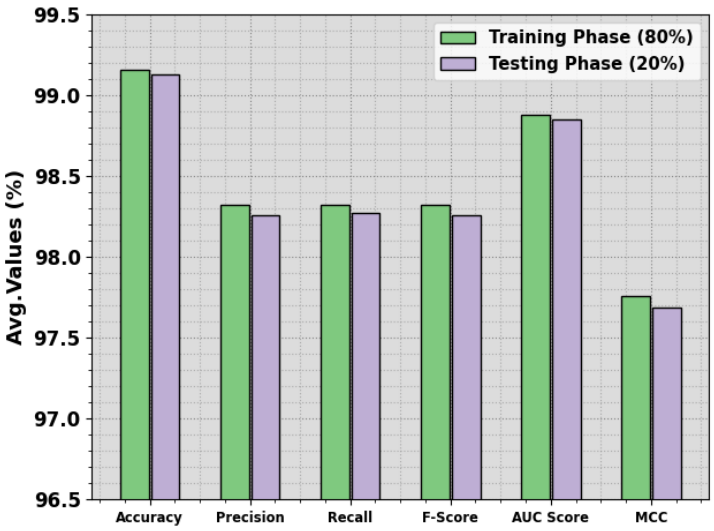

Figure 5. Average of CABTD-COAXAI technique at 80:20 of TRA phase/TES phase

The BT detection outcome of the CABTD-COAXAI algorithm is investigated under 70:30 of the TRA phase/TES phase in Table 3 and Figure 6. The outcome exhibits that the CABTD-COAXAI system achieves effective solution under each class. With 70% of the TRA phase, the CABTD-COAXAI algorithm offers an average $accu_y$ of 99.12%, $prec_n$ of 98.25%, $reca_l$ of 98.25%, F_{score} of 98.25%, AUC_{score} of 98.83%, and MCC of 97.66%. In the meantime, with 30% of the TES phase, the CABTD-COAXAI algorithm achieves an average $accu_y$ of 99.49%, $prec_n$ of 98.97%, $reca_l$ of 98.95%, F_{score} of 98.96%, AUC_{score} of 99.31%, and MCC of 98.62%.

Table 3: BT detection outcome of CABTD-COAXAI technique at 80:20 of TRA phase/TES phase

Classes	$Accu_y$	$Prec_n$	$Reca_l$	F_{Score}	AUC_{Score}	MCC
TRA phase (70%)						
Glioma	98.68	97.00	97.84	97.42	98.40	96.54
Meningioma	99.23	99.23	97.71	98.46	98.73	97.96
No-Tumor	99.42	98.89	98.78	98.84	99.21	98.45
Pituitary	99.15	97.89	98.66	98.27	98.98	97.71
Average	99.12	98.25	98.25	98.25	98.83	97.66
TES phase (30%)						
Glioma	99.29	98.66	98.40	98.53	98.99	98.06
Meningioma	99.36	99.21	98.17	98.68	98.96	98.26
No-Tumor	99.68	99.25	99.50	99.37	99.62	99.16
Pituitary	99.62	98.78	99.75	99.27	99.66	99.01
Average	99.49	98.97	98.95	98.96	99.31	98.62

To calculate the efficacy of the CABTD-COAXAI algorithm at 70:30 of the TRA phase/TES phase, we have created $accu_y$ curves for both the TRA and TES phases, as represented in Figure 7. These curves offer valued insights into the model's learning development and its capability to generalize. As we enhance the number of epochs, an obvious enhancement in both TRA and TES $accu_y$ curves develops apparently. This enhancement signifies the model's capacity to detect patterns within both the TRA and TES databases.

DOI: https://doi.org/10.54216/FPA.170203
Received: January 16, 2024 Revised: April 12, 2024 Accepted: September 13, 2024

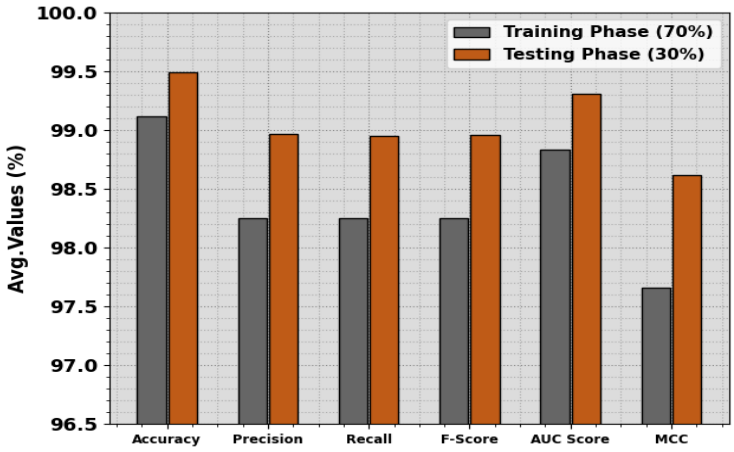

Figure 6. Average of CABTD-COAXAI technique at 70:30 of TRA phase/TES phase

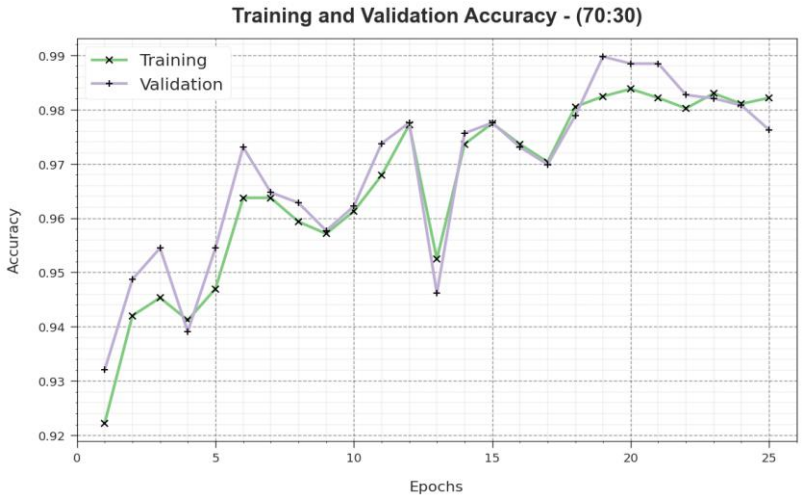

Figure 7. $Accu_y$ curve of CABTD-COAXAI technique at 70:30 of TRA phase/TES phase

Figure 8 also offers an overview of the CABTD-COAXAI technique at 70:30 of the TRA phase/TES phase, the loss values throughout the TRA model. The reducing trend in TRA loss over epochs indicates that the model continually refines its weights to decrease predictive errors on both TRA and TES data. This loss curve reflects how well the model fits the TRA data. Particularly, the TRA and TES losses consistently decrease, representing the model effective learning of designs present in both datasets. Moreover, it depicts the model's variation in decreasing discrepancies among predictions and the original TRA classes.

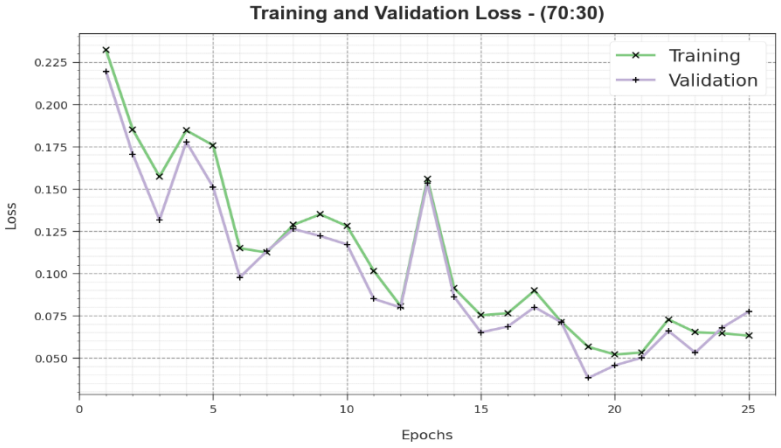

Figure 8. Loss curve of CABTD-COAXAI technique at 70:30 of TRA phase/TES phase

DOI: https://doi.org/10.54216/FPA.170203
Received: January 16, 2024 Revised: April 12, 2024 Accepted: September 13, 2024

The precision-recall outcome of the CABTD-COAXAI technique at 70:30 of the TRA phase/TES phase plots precision alongside recall as defined in Figure 9, revealing that our model gains superior precision-recall values across each class. This graph depicts the model's ability to detect various classes, especially excelling in correctly classifying positive instances but reducing false positives.

Figure 10 also contains ROC outcomes of the CABTD-COAXAI approach at 70:30 of the TRA phase/TES phase, which exhibits the model's ability to discriminate between class labels. These curves offer valuable insights into the exchange among true positive rates (TPR) as well as false positive rates (FPR) across various classification thresholds and epochs. They highlight the model's accurate predictive performance across various classes, underlining its classification abilities.

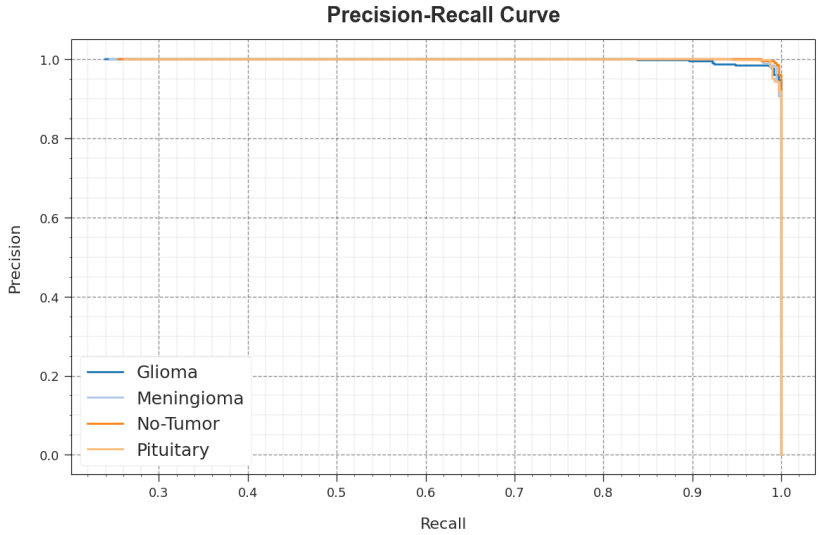

Figure 9. PR curve of CABTD-COAXAI technique at 70:30 of TRA phase/TES phase

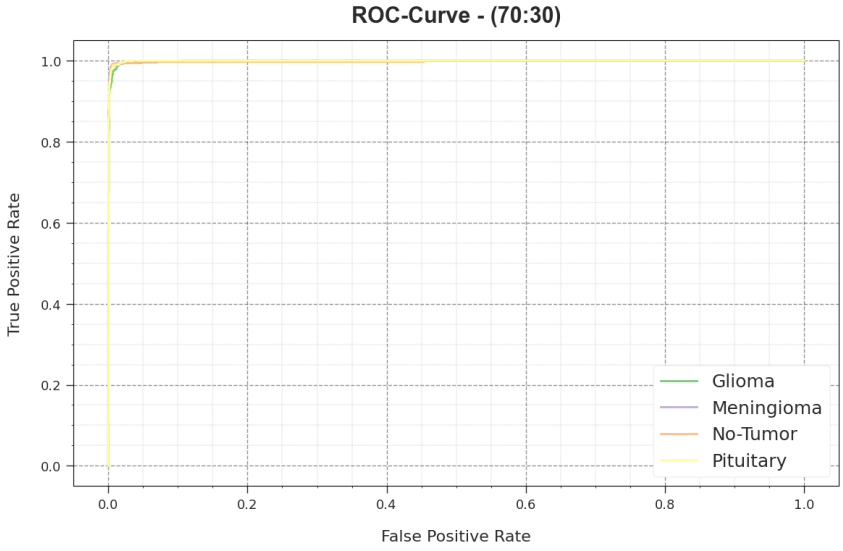

Figure 10. ROC curve of CABTD-COAXAI technique at 70:30 of TRA phase/TES phase

A detailed comparative study of the CABTD-COAXAI technique is studied in Table 4 and Figure 11 [25]. The results highlighted that the CABTD-COAXAI technique reaches a higher $accu_y$ of 99.49%. Contrastingly, the ELCAD-BTC, novel 2D-CNN, novel 3D-CNN, VGG19, Inceptionv3, 3D-CNN, and Fine-tuned VGG19 algorithm obtain decreased $accu_y$ values of 99.24%, 98%, 89.50%, 90.70%, 95.60%, 98.38%, and 94%, respectively.

DOI: https://doi.org/10.54216/FPA.170203
Received: January 16, 2024 Revised: April 12, 2024 Accepted: September 13, 2024

Table 4: $Accu_y$ outcome of CABTD-COAXAI technique with other approaches

Methods	Accuracy (%)
CABTD-COAXAI	99.49
ELCAD-BTC	99.24
Novel 2D-CNN	98.00
Novel 3D-CNN	89.50
VGG19 Model	90.70
InceptionV3	95.60
3D-CNN Model	98.38
Fine-tuned VGG19	94.00

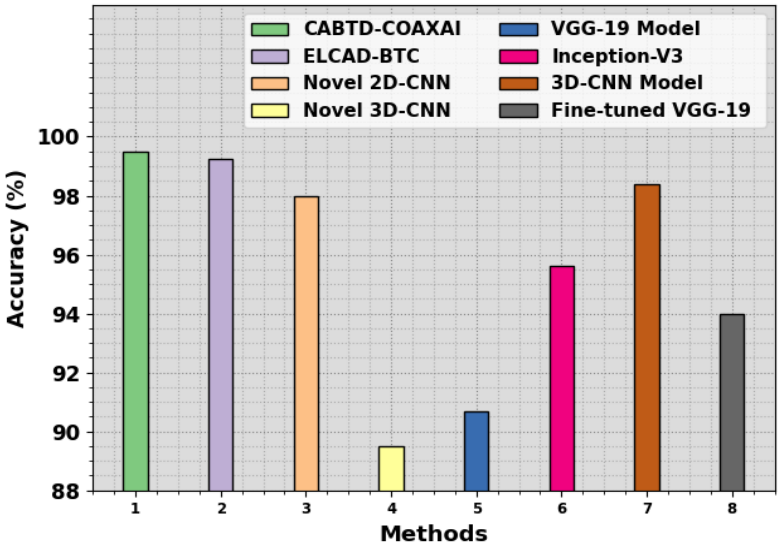

Figure 11. $Accu_y$ Outcome of CABTD-COAXAI technique with other approaches

In Table 5 and Figure 12, the computation time (CT) results of the CABTD-COAXAI technique are examined. The results indicate that the CABTD-COAXAI technique reaches a minimal CT of 1.13s. On the other hand, the ELCAD-BTC, Novel 2D-CNN, Novel 3D-CNN, VGG19 Model, InceptionV3, 3D-CNN Model, and Fine-tuned VGG-19 approaches obtain increased CT values. Thus, the CABTD-COAXAI technique can be employed for automated BT detection and classification processes.

Table 5 CT outcome of CABTD-COAXAI technique with other approaches

Methods	Computational Time (sec)
CABTD-COAXAI	1.13
ELCAD-BTC	4.83
Novel 2D-CNN	5.35
Novel 3D-CNN	2.02
VGG19 Model	5.60
InceptionV3	5.92
3D-CNN Model	2.52
Fine-tuned VGG-19	2.17

DOI: https://doi.org/10.54216/FPA.170203
Received: January 16, 2024 Revised: April 12, 2024 Accepted: September 13, 2024

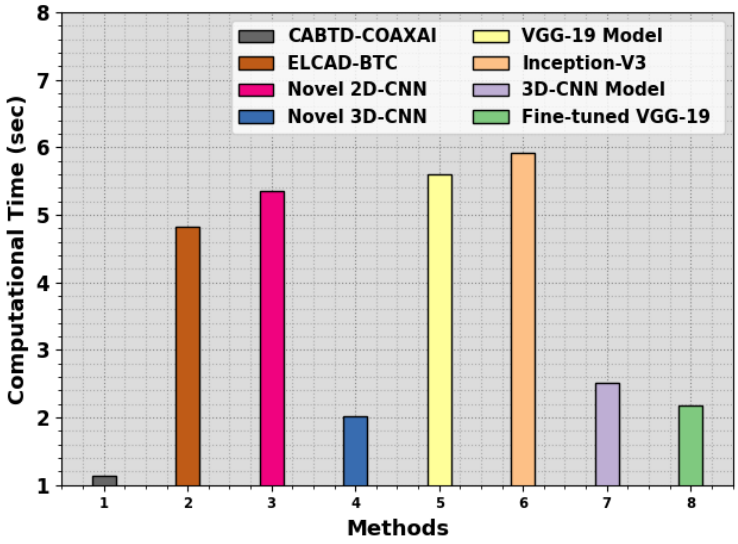

Figure 12. CT outcome of CABTD-COAXAI technique with other approaches

5. Conclusion

In this study, we concentrate on the design and development of the CABTD-COAXAI approach. The purpose of the CABTD-COAXAI technique is to exploit XAI and hyper parameter-tuned DL models for automated BT diagnosis. To accomplish this, the CABTD-COAXAI technique contains GF-pre-processing, EfficientNetB7-based feature extraction, COA-based parameter tuning, and CAE-based classification. To accomplish this, the CABTD-COAXAI technique follows GF based noise removal process. Additionally, the hyper parameter tuning of the EfficientNetB7 method is performed by the use of COA. Furthermore, the classification of the BT process can be performed by the usage of CAE. Finally, the CABTD-COAXAI system combines the XAI method named LIME to effectively understand and explain ability of the black-box model for automated BT diagnosis. The experimental result of the CABTD-COAXAI technique is tested on a benchmark BT database. The extensive outcomes inferred that the CABTD-COAXAI technique reaches superior performance over other models in terms of different measures.

Funding: "The author gratefully acknowledges technical support provided by the Faculty of Computing and Information Technology, King Abdulaziz University, Jeddah, Saudi Arabia"

Conflicts of Interest: "The authors declare no conflict of interest."

References

[1] Ahmed, F., Asif, M., Saleem, M., Mushtaq, U.F. and Imran, M., 2023. Identification and Prediction of Brain Tumor Using VGG-16 Empowered with Explainable Artificial Intelligence. International Journal of Computational and Innovative Sciences, 2(2), pp.24-33.

[2] Zeineldin, R.A., Karar, M.E., Elshaer, Z., Coburger, J., Wirtz, C.R., Burgert, O. and Mathis-Ullrich, F., 2022. Explainability of deep neural networks for MRI analysis of brain tumors. International journal of computer assisted radiology and surgery, 17(9), pp.1673-1683.

[3] Yu, L., Yu, Z., Sun, L., Zhu, L. and Geng, D., 2023. A brain tumor computer-aided diagnosis method with automatic lesion segmentation and ensemble decision strategy. Frontiers in Medicine, 10.

[4] Kalaiselvi, T. and Padmapriya, S.T., 2021. Brain tumor diagnostic system—a deep learning application. Machine Vision Inspection Systems, Volume 2: Machine Learning-Based Approaches, pp.69-90.

[5] Forghani, R., 2020. Precision digital oncology: emerging role of radiomics-based biomarkers and artificial intelligence for advanced imaging and characterization of brain tumors. Radiology: Imaging Cancer, 2(4), p.e190047.

[6] Gaur, L., Bhandari, M., Razdan, T., Mallik, S. and Zhao, Z., 2022. Explanation-driven deep learning model for prediction of brain tumour status using MRI image data. Frontiers in genetics, 13, p.448.

DOI: https://doi.org/10.54216/FPA.170203
Received: January 16, 2024 Revised: April 12, 2024 Accepted: September 13, 2024

[7] Hussain, T., Ullah, A., Haroon, U., Muhammad, K. and Baik, S.W., 2021. A comparative analysis of efficient CNN-based brain tumor classification models. In Generalization with deep learning: for improvement on sensing capability (pp. 259-278).

[8] Ali, S., Li, J., Pei, Y., Khurram, R., Rehman, K.U. and Mahmood, T., 2022. A comprehensive survey on brain tumor diagnosis using deep learning and emerging hybrid techniques with multi-modal MR image. Archives of computational methods in engineering, 29(7), pp.4871-4896.

[9] Kumar, A., Manikandan, R., Kose, U., Gupta, D. and Satapathy, S.C., 2021. Doctor's dilemma: evaluating an explainable subtractive spatial lightweight convolutional neural network for brain tumor diagnosis. ACM Transactions on Multimedia Computing, Communications, and Applications (TOMM), 17(3s), pp.1-26.

[10] Virupakshappa and Amarapur, B., 2020. Computer-aided diagnosis applied to MRI images of brain tumor using cognition based modified level set and optimized ANN classifier. Multimedia Tools and Applications, 79(5-6), pp.3571-3599.

[11] Benyamina, H., Mubarak, A.S. and Al-Turjman, F., 2022, October. Explainable Convolutional Neural Network for Brain Tumor Classification via MRI Images. In 2022 International Conference on Artificial Intelligence of Things and Crowdsensing (AIoTCs) (pp. 266-272). IEEE.

[12] Liu, T., Yuan, Z., Wu, L. and Badami, B., 2021. Optimal brain tumor diagnosis based on deep learning and balanced sparrow search algorithm. International Journal of Imaging Systems and Technology, 31(4), pp.1921-1935.

[13] Lu, S.Y., Satapathy, S.C., Wang, S.H. and Zhang, Y.D., 2021. PBTNet: a new computer-aided diagnosis system for detecting primary brain tumors. Frontiers in cell and developmental biology, 9, p.765654.

[14] Deepak, S. and Ameer, P.M., 2019. Brain tumor classification using deep CNN features via transfer learning. Computers in biology and medicine, 111, p.103345.

[15] Sadad, T., Rehman, A., Munir, A., Saba, T., Tariq, U., Ayesha, N. and Abbasi, R., 2021. Brain tumor detection and multi-classification using advanced deep learning techniques. Microscopy Research and Technique, 84(6), pp.1296-1308.

[16] Sajjad, M., Khan, S., Muhammad, K., Wu, W., Ullah, A. and Baik, S.W., 2019. Multi-grade brain tumor classification using deep CNN with extensive data augmentation. Journal of computational science, 30, pp.174-182.

[17] Noreen, N., Palaniappan, S., Qayyum, A., Ahmad, I., Imran, M. and Shoaib, M., 2020. A deep learning model based on concatenation approach for the diagnosis of brain tumor. IEEE Access, 8, pp.55135-55144.

[18] Dandıl, E. and Karaca, S., 2021. Detection of pseudo brain tumors via stacked LSTM neural networks using MR spectroscopy signals. Biocybernetics and Biomedical Engineering, 41(1), pp.173-195.

[19] Soares, L.B., da Costa, E.A.C. and Bampi, S., 2019, November. A configurable pruning Gaussian image filter for energy-efficient edge detection. In 2019 26th IEEE International Conference on Electronics, Circuits and Systems (ICECS) (pp. 666-669). IEEE.

[20] Huang, Z., Su, L., Wu, J. and Chen, Y., 2023. Rock Image Classification Based on EfficientNet and Triplet Attention Mechanism. Applied Sciences, 13(5), p.3180.

[21] Abou Houran, M., Bukhari, S.M.S., Zafar, M.H., Mansoor, M. and Chen, W., 2023. COA-CNN-LSTM: Coati optimization algorithm-based hybrid deep learning model for PV/wind power forecasting in smart grid applications. Applied Energy, 349, p.121638.

[22] Sadeghi-Adl, Z. and Ahmad, F., Semi-Supervised Convolutional Autoencoder With Attention Mechanism for Activity Recognition.

[23] Gashi, M., Vuković, M., Jekic, N., Thalmann, S., Holzinger, A., Jean-Quartier, C. and Jeanquartier, F., 2022. State-of-the-art explainability methods with focus on visual analytics showcased by glioma classification. BioMedInformatics, 2(1), pp.139-158.

[24] https://www.kaggle.com/datasets/masoudnickparvar/brain-tumor-mri-dataset

[25] Vaiyapuri, T., Jaiganesh, M., Ahmad, S., Abdeljaber, H.A., Yang, E. and Jeong, S.Y., 2023. Ensemble Learning Driven Computer-Aided Diagnosis Model for Brain Tumor Classification on Magnetic Resonance Imaging. IEEE Access.

DOI: https://doi.org/10.54216/FPA.170203
Received: January 16, 2024 Revised: April 12, 2024 Accepted: September 13, 2024